Luminescent Gold Nanocluster-Methylcellulose Composite Optical Fibers with Low Attenuation Coefficient and High Photostability

Hynninen, Ville

2021-07

Hynninen , V , Chandra , S , Das , S , Amini , M , Dai , Y , Lepikko , S , Mohammadi , P , Hietala , S , Ras , R H A , Sun , Z , Ikkala , O & Nonappa , D 2021 , ' Luminescent Gold Nanocluster-Methylcellulose Composite Optical Fibers with Low Attenuation Coefficient and High Photostability ' , Small , vol. 17 , no. 27 , 2005205 . https://doi.org/10.1002/smll.202005205

http://hdl.handle.net/10138/341189
https://doi.org/10.1002/smll.202005205

unspecified
acceptedVersion

Luminescent Gold Nanocluster-Methylcellulose Hybrid Optical Fibers with Low Attenuation Coefficient and High Photostability

Ville Hynninen, Sourov Chandra, Susobhan Das, Mohammad Amini, Yunyun Dai, Sakari Lepikko, Pezhman Mohammadi, Sami Hietala, Robin H. A. Ras, Zhipei Sun, Olli Ikkala, Nonappa**

V. Hynninen, Prof. Nonappa
Faculty of Engineering and Natural Sciences, Tampere University
P.O. Box 541, FI-33101 Tampere, Finland
E-mail: nonappa@tuni.fi

V. Hynninen, Dr. S. Chandra, S. Lepikko, Prof. R. H. A. Ras, Prof. O. Ikkala, Prof. Nonappa
HYBER Centre of Excellence, Department of Applied Physics
Aalto University, P. O. Box 15100, FI-00076, Espoo, Finland
E-mail: olli.ikkala@aalto.fi

Dr. S. Das, M. Amini, Dr. Y. Dai, Prof. Z. Sun
Department of Electronics and Nanoengineering, Aalto University
Tietotie 3, FI-02150, Espoo, Finland

Dr. S. Das, M. Amini, Dr. Y. Dai, Prof. Z. Sun
QTF Centre of Excellence, Department of Applied Physics, Aalto University, FI-00076, Espoo, Finland

Dr. P. Mohammadi
VTT Technical Research Centre, P.O. Box 1000, FI-02044, Espoo, Finland

Dr. S. Hietala
Department of Chemistry, University of Helsinki P.O. Box 55, FI-00014, Helsinki, Finland.

Abstract:

Because of their lightweight structure, flexibility, and immunity to electromagnetic interference, polymer optical fibers (POFs) have been used in numerous short-distance applications. Notably, the incorporation of luminescent nanomaterials in POFs offers optical amplification for advanced nanophotonics. However, conventional POFs suffer from non-sustainable components and processes. Furthermore, the traditionally used luminescent nanomaterials undergo photobleaching, oxidation and can be cytotoxic. Therefore, biopolymer-based optical fibers containing non-toxic luminescent nanomaterials are needed, with efficient and environmentally acceptable extrusion methods. Here, we demonstrate such an approach

for fibers wet-spun from shear-thinning aqueous methylcellulose (MC) dispersions and composite hydrogels. Using cut-back attenuation measurement, we show that the resulting fibers are capable of acting as short-distance optical fibers with attenuation coefficient as low as 1.47 dB cm^{-1}. To study the effect of mechanical reinforcement and types of nanomaterials, *viz*, cellulose nanocrystals (CNCs), glutathione capped gold nanoclusters (Au@GSH), Au@GSH covalently linked to CNCs (CNC-Au@GSH), and bovine serum albumin coated were used. This is on par with or even lower than some of the previously reported biopolymeric optical fibers, even with optical cladding. Importantly, the gold nanoclusters retain their intrinsic luminescence and sensing abilities even upon incorporation in the MC matrix. The hybrid optical fibers show high photostability encouraging the design of short-distance degradable optical fibers and sensors.

1.0 Introduction

Optical fibers are the current mainstream choice for fast and high-capacity communication networks. The state-of-the-art single mode silica glass optical fibers (GOFs) have an attenuation coefficient of ca. 0.2 dB km^{-1}, i.e., they can carry signals over tens of kilometers without significant losses or need for amplification.[1] However, they are not optimal for certain short-distance technologies due to their brittleness, lack of flexibility, poor modifiability, and lack of biocompatibility, such as in selected automotive, household networks, smart textile, and biosensor applications.[2] By contrast, multimode polymeric optical fibers, aka plastic optical fibers (POFs), have the potential to overcome such limitations. They are cost-effective and offer mechanical softness and ductility. The synthetic POFs typically consists of a high refractive index (RI) poly(methyl methacrylate) (PMMA, RI ~1.49) or polystyrene (PS, RI ~1.56) core surrounded by a low refractive index fluorinated polymer (RI ~1.35) cladding. POFs under appropriate composition and chemical modification allow the incorporation of functional dopants in their matrix.[3–6] POFs have been exploited as matrices for various dopants, including

dye molecules (e.g., rhodamine B, rhodamine 6G and perylene),[7] noble metal nanoparticles,[8] quantum dots,[9] and rare earth metal ions.[10] Functional dopants allow optical amplification for nanophotonic applications. Nanoparticle doped composite fibers have been utilized as sensors,[11] wearable and stretchable devices,[12] and for inactivation of bacteria.[13] However, most of the existing luminescent dye molecules and nanomaterials are prone to photobleaching, oxidation, and are cytotoxic.[14-18] Importantly, commercial POFs display inherently higher attenuation coefficients (0.16 dB m^{-1} to 0.30 dB m^{-1}) compared to that of GOFs. Moreover, POFs allow the manufacturing of thicker multimode fibers with increased signal dispersion.[5,19] Nevertheless, the low attenuation coefficient of POFs is acceptable in short length scale devices. However, they tend to be environmentally compromised, e.g., due to high temperature processing, toxic or hazardous chemical treatments, and limited biodegradability.[20–22]

Biopolymers such as agarose and alginate-based hydrogels,[23–26] gelatin,[27,28] chitosan,[29-31] silk,[32–36] and DNA,[37,38] have been studied for optical waveguides. Among biopolymers, cellulose-based materials offer several components with refractive indices between 1.51 and 1.47, making them suitable for uniform refractive index optical fibers. Rather surprisingly, even if being a renewable and sustainable natural polymer, cellulose has not been broadly explored for fiber optics.[39] Nevertheless, cellulose and nanocellulose based materials for other photonic applications have been studied and reviewed in the literature.[40-52] To date, only two reports of fully cellulose-derived optical fibers exist, i.e., prepared from hydroxypropyl cellulose (HPC) -filled cellulose butyrate (CB) tubes and cellulose acetate (CA) coated regenerated cellulose fibers, respectively.[53,54] The preparation of these fibers still involves high temperature treatment and the use of ionic liquids. Among cellulose derivatives, methylcellulose (MC) is a well-known charge-neutral polymer (RI ~1.49) that has been studied as a potential alternative for oil-based polymers. It has been used in several applications, including foods, detergents, paints, adhesives, cosmetics, pharmaceuticals, and functional gels.[55–57] MC is a water-dispersible polymer (**Figure 1**a) that shows lower critical solution temperature (LCST)

behavior, i.e., it forms turbid hydrogels at elevated temperatures (**Figure 1**a, b).[58–60] Upon gelation, MC polymers self-assemble into fibrillar bundles and increase the gel stiffness. The mechanical properties of the MC polymer network can be altered by adding nanoparticles, such as cellulose nanocrystals (CNCs) or chitin nanocrystals.[57–59]

Among noble metal nanoparticles, atomically precise gold nanoclusters (GNCs) have gained considerable attention as luminescent nanomaterials.[61- 65] Their small size, water soluble nature, and molecule-like optoelectronic properties readily allow dispersion in hydrogels.[66] Besides, certain GNCs are highly fluorescent, photostable, non-toxic and biocompatible. GNCs also possess a high surface-to-volume ratio, excellent catalytic potential and acts as sensors for heavy metal ion detection.[61-66] Among all studied luminescent gold nanoclusters, bovine serum albumin (BSA) coated gold nanoclusters (GNC-BSA) and reduced glutathione (GSH) capped gold nanoclusters(GNC-GSH) have been explored for sensors, catalysis, bioimaging and pathogen detection.[67-79] Despite tremendous progress in luminescent GNCs, their incorporation in biopolymeric fibers for optical amplification and waveguiding is unexplored to date.

Here we use shear thinning aqueous methylcellulose (MC) dispersions and composite hydrogels to wet-spin fibers under ambient conditions without any hazardous chemicals or treatment. For the preparation of nanocomposite hydrogel-based fibers, four types of nanoparticles were used, *viz*., (i) bovine serum albumin encapsulated gold nanocluster (GNC-BSA), (ii) glutathione capped gold nanoclusters (GNC-GSH), (iii) GNC-GSH covalently linked to cellulose nanocrystals (CNC-GNC), and (iv) cellulose nanocrystals (CNCs) were used. We demonstrate the effect of hydrogel solid content and dopants on fiber mechanical properties, optical properties and the attenuation coefficients. Finally, we show that the GNCs retain their intrinsic optoelectronic properties and metal ion sensing abilities with enhanced photostability under continuous ultraviolet (UV) light irradiation and temperature dependent degradation in an aqueous environment.

2.0 Results and Discussion

2.1 Preparation and characterization of GNCs, CNCs and the hybrid CNC-GNCs

Figure 1 summarizes the materials used for the preparation of MC-nanoparticle composite optical fibers. The aqueous dispersions of commercial MC polymer (MW 88000 g/mol, degree of substitution ~ 1.5-1.9) were prepared according to reported literature procedures (**Figure 1**a**,** b).[80,81] The synthesis of GNC-BSA and GNC-GSH were carried out using $HAuCl_4.3H_2O$ in the presence of BSA and GSH ligands, respectively (**Figure 1**c).[72] The sulfuric acid hydrolysis method was used to prepare cellulose nanocrystals (CNCs) with an average length of 238 nm, and aspect ratio of ca. 14 with sulfate half ester content of 239 μmol g^{-1} (**Figures 1**c , **S**1).[80,81] The GNCs attached to the CNC surface (CNC-GNC), were synthesized by adding the precursor ($HAuCl_4.3H_2O$) to an aqueous CNC suspension followed by the addition of GSH ligands. The TEM image of CNC-GNCs displayed an inter-nanocluster distance of ~ 5 nm over the CNC surface (**Figure 1**c). The presence of Au, C, O and two different types of S atoms in CNC-GNCs was determined using energy dispersive X-ray (EDX) and X-ray photoelectron spectroscopy (XPS) analysis (**Figures S2, S3**). The XPS spectrum corresponding to S2p3/2 appeared as a single peak at 169.2 eV for CNCs (**Figure S**3b). However, for CNC-GNCs, an additional peak at lower oxidation state at around 163.1 eV was also observed due to the presence of, (i) the $-OSO_3^-$ groups in CNCs and (ii) -SH groups from GSH over the surface of the GNC-GSH. The Au4f7/2 XPS spectrum of CNC-GNC confirmed typical peak positions of gold nanoclusters with Au(0) core and Au(I) surfaces at 83.9 eV and 84.8 eV, respectively (**Figure S3**c).[72]

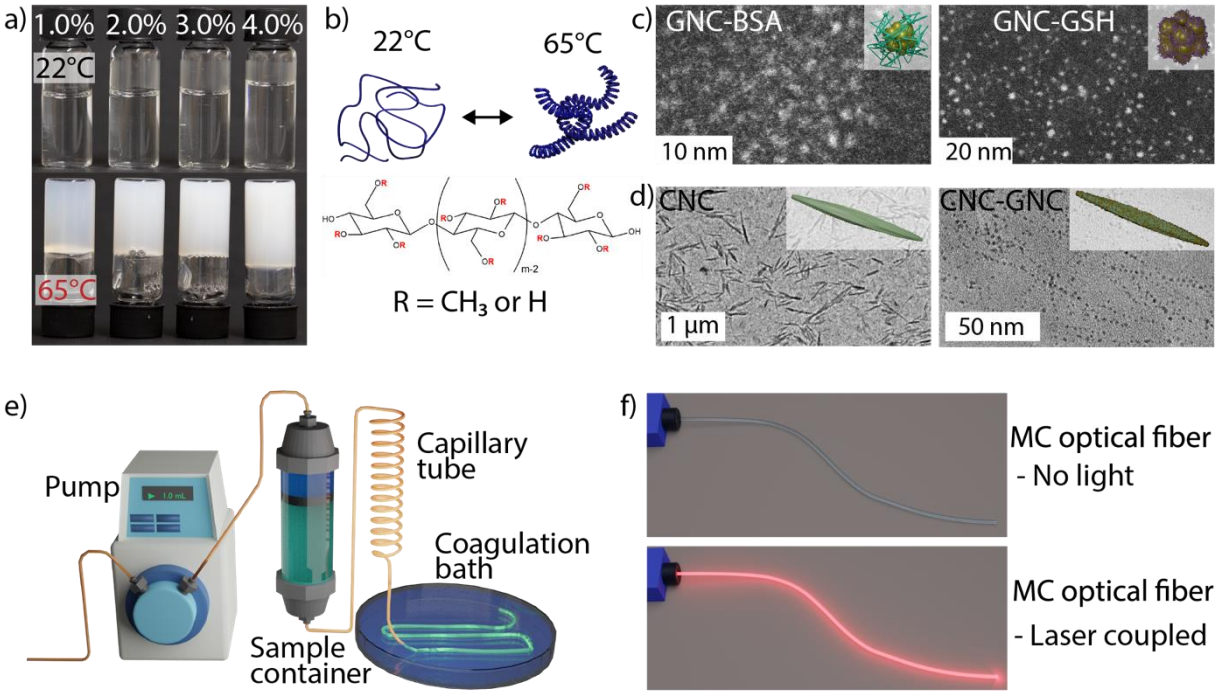

Figure 1. Materials and methods used in this study. a) Photographs of 1, 2, 3 and 4 w/v% of MC aqueous solutions at 22 °C (top) and gels at 65 °C (bottom). b) Schematic representation showing a random coil-to-fibrillar structural transition of MC polymers upon heating. c) Darkfield (DF) STEM images and schematic (inset) drawings of GNC-BSA (left), GNC-GSH (right). d) TEM images of CNCs (left) and CNC-GNCs (right). e) Schematic illustration of fiber extrusion equipment. f) Schematic representation of the biopolymeric fibers without (top) and with coupling a light source (bottom).

The GNC-BSA and GNC-GSH showed the characteristic absorption peaks at 520 nm and 400 nm, respectively in UV-vis absorbance spectra (**Figure 2**a, see the experimental section for details). However, the characteristic absorbance spectral feature was not observed for GNC-GSH covalently attached to CNCs (GNC-CNC). The lack of absornace spectral features is presumably due to the relatively high CNC content compared to GNC-GSH, and possible overlapping absorption regions of the components. The photoluminescence excitation (PLE) spectrum at 600 nm emission showed an analogous broad peak centered around 390 nm for both GNC-GSH and CNC-GNC (**Figure 2**b). This suggests that in CNC-GNCs, the optical property of GNC-GSH was well retained after binding with the surface of CNCs. The PL emission spectra of GNC-BSA and GNC-GSH showed broad peaks centered at 660 nm (at λ_{ex} = 470 nm) and 590 nm (at λ_{ex} = 400 nm), respectively (**Figure 2**c). Importantly, for CNC-GNCs,

the position of PL emission peak corresponding to GNC-GSH was unaltered after chemically binding with CNCs (**Figure 2**c) and showed strong fluorescence under UV-irradiation (**Figure 2**d).

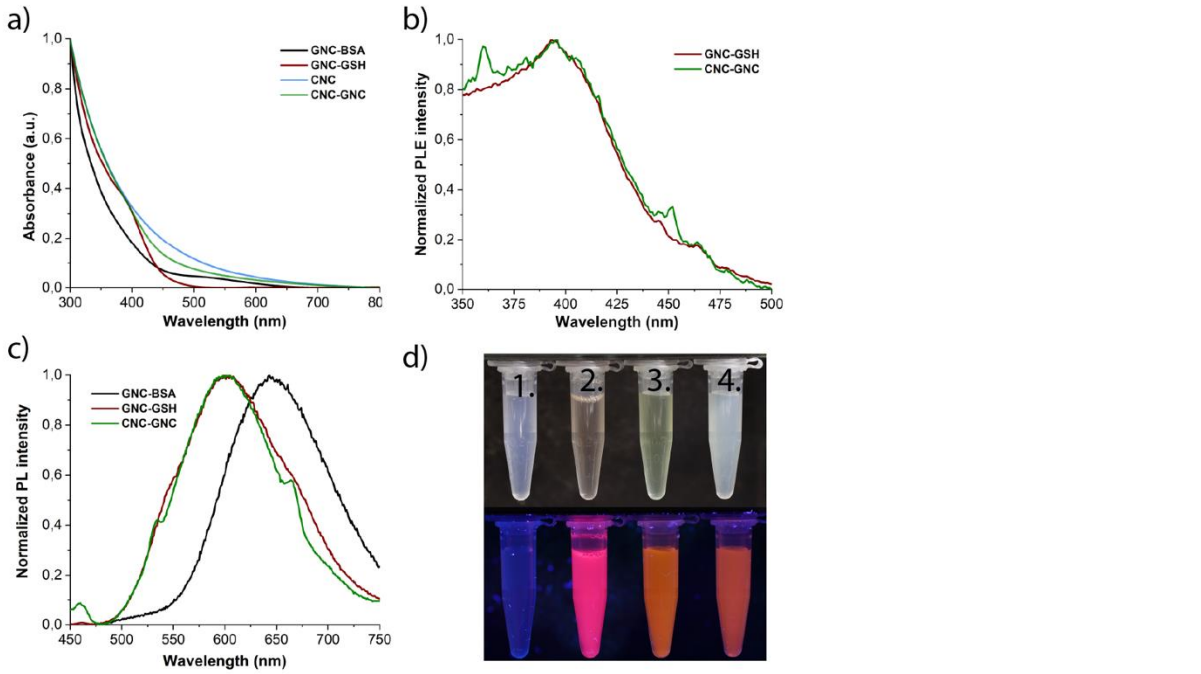

Figure 2. Optical properties of GNCs. a) UV-vis absorption spectra of aqueous GNCs, CNC and GNC-CNC dispersions. b) Photoluminescence excitation spectra of GNC-GSH and CNC-GNC. c) Photoluminescence emission spectra of GNCs. d) Photographs of aqueous dispersions of the nanoparticles at ambient conditions (above) and under UV light (below): 1) 1.0% CNCs, 2) 1.0% GNC-BSA, 3) 0.04% GNC-GSH, 4) (a) 1.0% CNC-GNC.

2.2 Rheological properties of MC dispersions and composite hydrogels.

To determine the optimal MC concentration suitable for wet-spinning, strain sweep, frequency sweep and shear viscosities were determined using oscillatory rheological measurements at 22 ^{o}C (**Figure 3**). Accordingly, the baseline MC concentration range between 2.0-4.0% (note: all % refers to weight of the solid/volume of the solvent, i.e., w/v%) was selected. The strain sweep experiments of pure MC aqueous dispersions (2.0 -4.0%) displayed loss modulus (*G´´)* higher than storage modulus (*G´*) as expected for viscous fluids (**Figure 3**a). This suggests that all the MC dispersions are liquid-like under the experimental conditions. The storage modulus (*G´*) increased considerably with increasing concentration of MC solid content. For example, 2.0%,

3.0% and 4.0% MC dispersions showed *G´* values of 7, 43 and 154 Pa, respectively. The frequency sweep experiments show that the loss modulus (*G´´*) remained above storage modulus (*G´*), and the frequency-dependency of *G´* i.e., at low frequency *G´´*> *G´* and at high angular frequency *G´*> *G´´* (**Figure 3**b). Importantly, the *G´* and *G´´* slopes of all MC samples are roughly similar, thus suggesting that the systems are, in fact, close to sol-gel transition state. The viscosity increased with the increasing MC solid content from 8, 25 and 105 Pa.s, for 2.0, 3.0 and 4.0% MC, respectively (**Figure 3**c). Shear-rate dependent decreasing viscosity, i.e., shear thinning, was observed for all compositions, which is considered beneficial for wet-spinning.

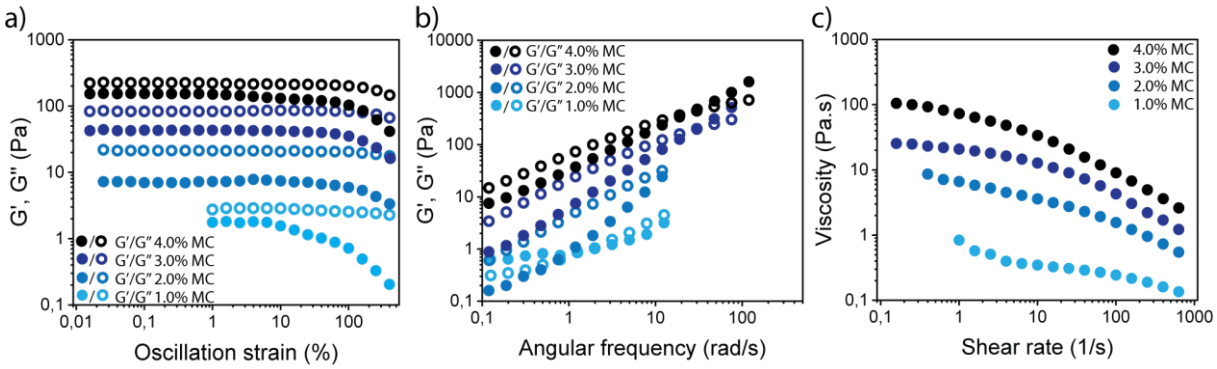

Figure 3. Rheological characterization of MC aqueous dispersions. a) Strain sweeps, b) frequency sweeps, and c) steady-shear flow sweeps of 1.0, 2.0, 3.0 and 4.0% MC aqueous dispersions.

Next, the effect of dopants on the rheological properties of the MC systems was explored. We first used a ratio of 3.0% MC to 0.75% dopants (i.e., 4:1 solid content ratio, w/w%), since this composition was shown to achieve good mechanical properties previously for MC/CNC nanocomposite hydrogels.[81] Macroscopically, all compositions displayed resistance to flow upon vial inversion. However, under rheological measurements, the MC/GNC-BSA, MC/GNC-GSH displayed liquid-like behavior at all the studied compositions, similar to that of pure MC dispersions (**Figure 4**). The MC/CNC-GNC, MC/CNC and a three-component mixture of MC/CNC/GNC-BSA all displayed gel-like rheological properties with *G´*>*G´´*. The

representative strain sweep and shear viscosity of MC/GNC-BSA and MC/GNC-GSH are presented in Figure 4. The storage modulus, *G´* of MC/GNC-BSA (3.0/0.75 w/w) was slightly higher (52 Pa) than that of pure 3.0% MC, presumably due to an increase in the solid content. However, for MC/GNC-BSA 3.0/1.0 composition (i.e., the overall solid content 4.0%), the *G´* was found to be similar to 3.0/0.75 composition. This suggests the limited mechanical reinforcement of composite gels by GNC-BSA.

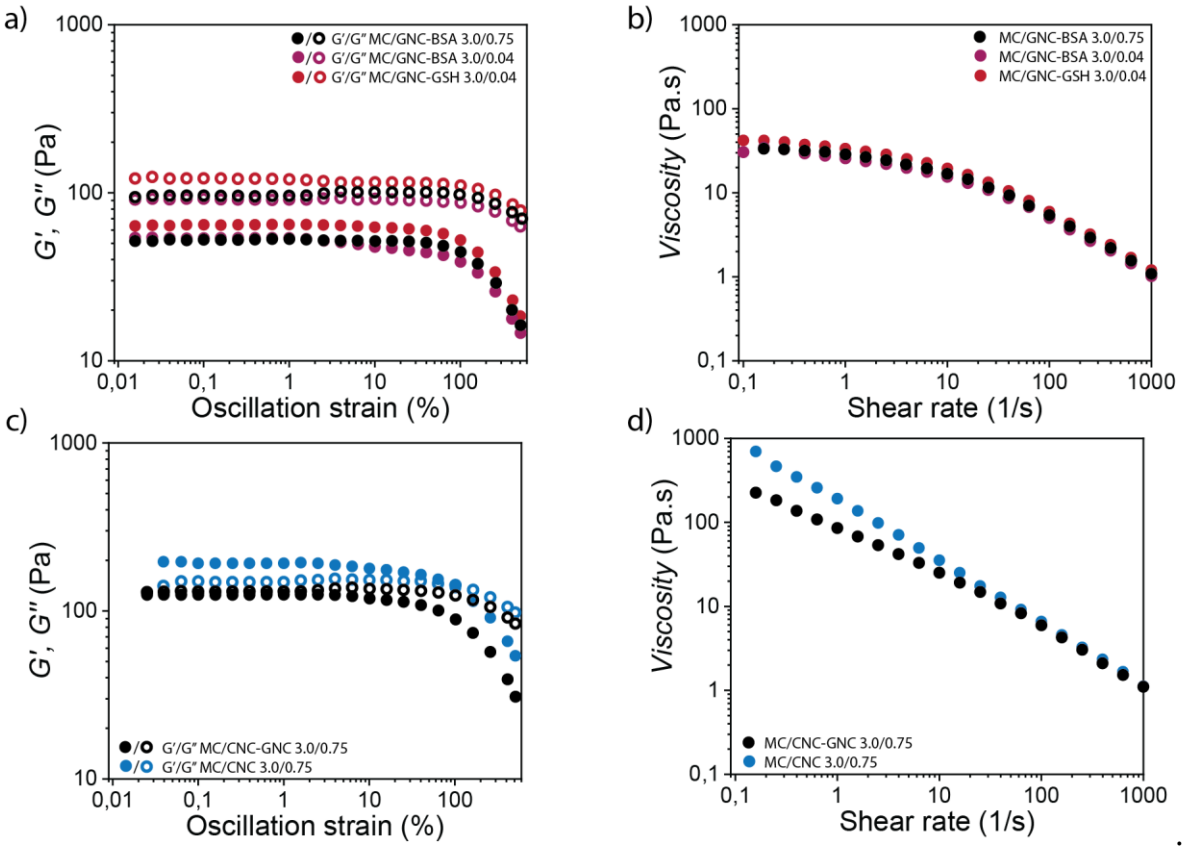

Figure 4. Rheological properties of MC nanocomposite dispersions and hydrogels. a,b) Strain sweeps and flow sweeps of MC-GNC nanocomposites. c,d) Strain sweeps and flow sweeps of CNC and GNC containing MC nanocomposites.

Furthermore, keeping the overall solid content identical but altering the weight ratio of MC-to-GNC-BSA from 3:1 to either 2:2 or 1.4:2.6, further reduced the hydrogel modulus. This suggests that 3.0% MC is close to an optimum concentration. Therefore, the amount of GNCs that maintains the mechanical properties of the composites close to that of 3.0% MC were optimized. For example, 3.0/0.04 MC/GNC-BSA composition displayed G´ of 41 Pa and the

viscosity of 34 Pa.s, which are similar to that of pure 3.0% MC. Similar experiments with the MC/GNC-GSH 3.0/0.04 composition showed slightly higher storage modulus (64 Pa) and viscosity (54 Pa.s). Interestingly, such a low loading of GNC was enough to impart luminescence to the composite systems.

The MC/CNC-GNC having a composition of 3.0/0.75 displayed near gel-like properties (G' ≈ G'') with low strain limit *G´* value of 125 Pa (**Figure 4**c, d). However, the storage modulus *G´* remained lower than that of pure 4.0% MC (154 Pa). In CNC-GNC hybrids, only a fraction (~2.6%) of the total mass corresponds to GNC-GSHs. In comparison, MC/CNC 3.0/0.75 showed low strain limit *G´* of 194 Pa and viscosity of 622 Pa.s indicative of significant stiffening accompanied with distinct gel-like characteristics of *G´ > G´´* and frequency-independent *G´* scaling (**Figure 4**c,d). Similar CNC-induced strengthening compared to pure MC hydrogels appeared with lower total solid content samples of MC/CNC 1.0/0.25 and MC/CNC 2.0/0.50 (**Figure S**7). A second control sample containing MC/BSA 3.0/0.75 displayed higher *G´* and viscosity (68 Pa and 56 Pa.s, respectively) compared to the MC/GNC-BSA 3.0/0.75 (**Figures S**4, **S**5). This is expected since under GNC synthesis conditions, BSA undergoes structural changes compared to native BSA. Finally, a three-component control system with a composition of MC/CNC/GNC-BSA 3.0/0.73/0.02 behaved similar to MC/CNC 3.0/0.75 control in its rheological behavior (**Figures S**4, **S**5). This is logical considering somewhat identical CNC content, giving no benefit for the covalently coupled MC/CNC-GNCs 3.0/0.75. In the literature, highly elongated anisotropic nanofillers have been demonstrated to yield higher mechanical reinforcement compared to smaller spherical particles.[82] Overall, considering the general size and shape of GNCs and CNCs and their hybrids, the observed relative behavior is in agreement with the existing literature.

2.3 Fiber spinning and morphology

MC-based hydrogels were wet-spun into solid fibers by extrusion through a capillary tube (ø = 1 mm, length = 1 m) into a coagulation bath filled with ethanol (96.0 v/v%) at 22 °C

(**Figure 1**d, see Experimental section for details).[81,82] The resulting fibers were structurally uniform, smooth and transparent (**Figure 5**). However, due to relatively low overall solid content, the gravity-driven flattening during the coagulation resulted in fibers with non-cylindrical and folded cross-sections (**Figure 5e, f** and **S8, S9**). The pure MC-based fibers were highly transparent with a glass-like appearance. The addition of dopants slightly altered the appearance and transparency of the fibers. MC/GNC-BSA fibers displayed pale reddish hue at low GNC-BSA concentration but turned red and opaque at higher concentrations (**Figures 5** and **S10**). MC/GNC-GSH and MC/CNC-GNC compositions produced yellowish and non-transparent fibers. Importantly, nanocomposite fibers with sufficient GNC loadings displayed luminescence under UV irradiation (**Figures 5**c, d and **S10**). The scanning electron microscopy (SEM) images of the fibers revealed the smooth surface morphology. The SEM images of fractured fiber cross-sections, showed oriented assemblies of rod-like internal building blocks to radiate from fiber's core towards the edges conforming to the overall cross-sectional shape (**Figure 5**g and **S11**). The rod-like building blocks have been earlier proposed to consist of hybrids of MC and CNCs in MC/CNC fibers. Here, the blocks were also observed in pure MC fibers, showing that they inherently stem from the MC component.[81] Thus, similar nanoscale internal features were observed in all fibers regardless of the composition due to dominating MC volume fraction, and no obvious internal structural differences between compositions appeared.

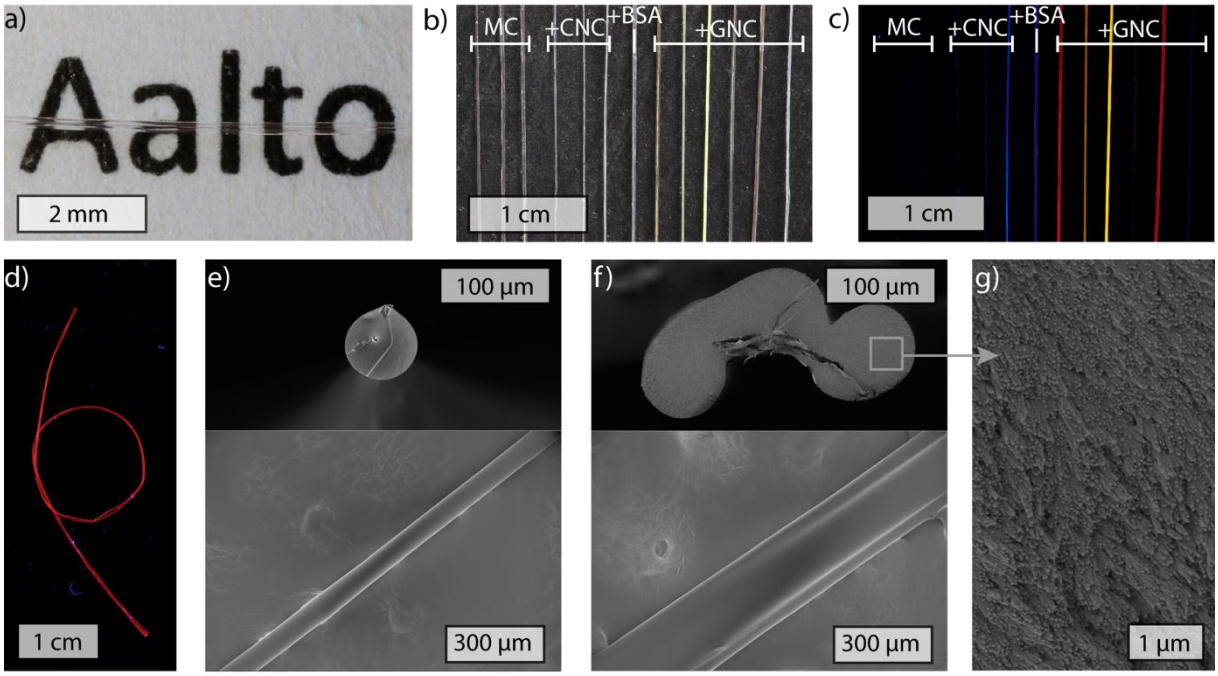

Figure 5. Morphology of MC-based optical fibers. a) Photograph showing a highly transparent MC 3.0 fiber placed on a printed text. b) Photographs of MC-based nanocomposite fibers of various compositions. Fibers from left to right are: MC 2.0, MC 3.0, MC 4.0, MC/CNC 1.0/0.25, MC/CNC 2.0 /0.50, MC/CNC 3.0/0.75, MC/BSA 3.0/0.75, MC/GNC-BSA 3.0/075, MC/CNC-GNC 3.0/0.75, MC/GNC-GSH 3.0/0.04, MC/GNC-BSA 3.0/0.04, MC/CNC/GNC-BSA 3.0/0.375/0.375, and MC/CNC/GNC-BSA 3.0/0.73/0.02. c) The same fibers as in (b) photographed under UV light. Fibers with GNCs show strong fluorescence except for low concentration MC/GNC-BSA3.0/0.04 fibers. MC/BSA control also shows some fluorescence, while MC and thinner MC/CNC fibers appear fully non-fluorescent. d) MC/GNC-BSA 3.0/0.75 shows intense photoluminescence under UV light and allows significant bending without breaking. e) SEM images of the fractured cross section and side view of and MC 2.0 fiber. f) SEM images of the fractured cross-section and side view of and MC 4.0 fiber. g) Close-up of the MC 4.0 fiber cross-sectional surface showing rod-like internal features characteristic for wet-spun MC-based fibers.

2.4 Fiber mechanical performance

Uniaxial tensile tests were performed to determine the mechanical properties of the wet-spun fibers. Typical average mechanical values (maximum stress, maximum strain, Young's modulus, and modulus of toughness) for selected fiber compositions are given in Table 1 (see Table S1 for complete mechanical testing data). Pure MC fibers showed an increasing trend in maximum strength and stiffness with increasing total solid content (**Figure 6**a). For example, an average maximum strength of 97.1, 109.4 and 151.7 MPa were observed from MC 2.0, MC 3.0 and MC 4.0, respectively. However, at the same time, the maximum strain decreased from

52.4% to 32.2% when going from MC 2.0 to MC 4.0 fibers. The modulus of toughness remained rather constant regardless of the MC content. Overall, MC 2.0 fibers achieved the highest maximum strain of all the tested compositions and it can be considered significantly high for a cellulose-based fiber.[86] On the other hand, MC 4.0 fibers appeared very competitive against the other known fully cellulose-derived optical fibers up to date, and lost only in stiffness compared to the CA-clad regenerated cellulose fibers that have showed a tensile strength of 129 MPa, the maximum strain of 21% and Young's modulus of 5.4 GPa.[53] The low MC content was deduced to allow low-density looser packing, which enabled enhanced ductility, while higher MC content became more densely packed, resulting in high stiffness but reduced flexibility.

Table 1. Representative mechanical properties of selected MC-based fibers.

Fiber composition	Max stress [MPa]	Max strain [%]	Young's modulus [GPa]	Modulus of toughness [MJ m^{-3}]
MC 3.0	109.4 ± 56.9	47.6 ± 16.5	2.6 ± 1.2	31.8 ± 18.7
MC 4.0	151.7 ± 33.0	32.2 ± 7.3	4.0 ± 0.4	31.5 ± 11.5
MC/GNC-BSA 3.0/0.75	127.6 ± 15.9	34.9 ± 7.8	4.0 ± 0.4	29.9 ± 9.3
MC/BSA 3.0/0.75	126.8 ± 28.6	35.6 ± 5.1	3.4 ± 0.7	29.5 ± 9.5
MC/GNC-BSA 3.0/0.04	160.0 ± 33.5	34.1 ± 7.5	4.1 ± 0.4	35.8 ± 13.1
MC/GNC-GSH 3.0/0.04	161.9 ± 27.7	45.1 ± 11.4	4.1 ± 0.3	48.9 ± 17.8
MC/CNC-GNC 3.0/0.75	161.6 ± 14.9	43.8 ± 6.9	5.4 ± 0.5	47.8 ± 10.1
MC/CNC/GNC-BSA 3.0/0.73/0.02	173.4 ± 24.9	43.4 ± 6.3	6.1 ± 0.5	52 ± 12.2

MC/CNC/GNC-BSA 3.0/0.375/0.375	154.8 ± 26.5	37.5 ± 9.8	5.0 ± 0.8	38.8 ± 14.9
MC/CNC 3.0/0.75	173.0 ± 19.5	33.8 ± 6.4	8.3 ± 1.1	41.4 ± 10.0

The mechanical properties of GNC-doped MC-composite fibers mostly followed their observed relative rheological behavior in the liquid state (**Figure 6**a). MC/GNC-BSA 3.0/0.75 fibers positioned itself in between MC 3.0 and MC 4.0 (**Table 1** and **Figure 6**b), likely due to an increased solid content but stronger than MC/BSA 3.0/0.75 control (**Figure 6**c). This suggests that in its dried state, the GNC-BSAs would be able to better provide relatively better reinforcement to the composite fibers compared to free BSA protein. This is attributed to fact that in the GNC-BSA, their rigid metal core could efficiently induce semi-stiff surrounding interfacial regions and contribute to the overall material stiffness compared to the gel-state.[83] This kind of polymer-filler interaction-derived reinforcement mechanism has also been reported for CNC nanocomposites.[84,85] Furthermore, adjusting the MC-to-GNC-BSA ratio more towards the GNC-BSA resulted in weaker, softer and more ductile fibers, which is in agreement with their rheological behavior of the corresponding gels (**Figure S12**).

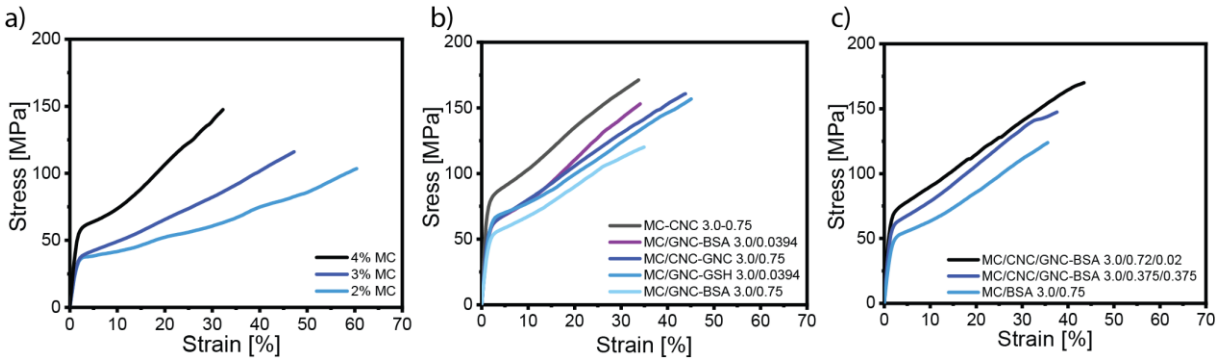

Figure 6. Tensile test performance of MC-based fibers. a) Representative stress-strain curves of pure MC fibers. b) Stress-strain curves of nanoparticle-doped MC/GNC-BSA, MC/CNC-GNC and MC/CNC composite fibers. c) Stress-strain curves of MC/BSA control and the three-component MC/CNC/GNC-BSA composite fibers.

Rather surprisingly, the composite fibers with very low GNC-BSA and GNC-GSH loadings of 0.04% demonstrated surprisingly strong mechanical enhancement. The MC/GNC-GSH 3.0/0.04 fibers showed maximum stress of 162 MPa, the maximum strain of 45.1%, Young's modulus of 4.1 GPa and toughness of 48.9 MJ m^{-3}. The fibers with MC/GNC-BSA 3.0/0.04 composition showed maximum strain of 160 MPa, strain of 34.1%, modulus of 4.1 GPa, and toughness of 35.8 MJ m^{-3}. Importantly, these two composite fibers outperformed the pure MC 4.0 fibers in all mechanical aspects regardless their ~25% lower overall solid content. This suggests that the mechanical benefits of the GNCs also in dry composites are best exploited at minimal loadings. However, 0.04% GNC-BSA loading was not sufficient impart luminescence, to the composite fibers. On the other hand, 0.04% GNC-GSH doped fibers were strongly fluorescent but turned opaque. The observed difference between the two types of GNC-doped fibers is presumably due to the different ligand coatings. Similarly, MC/CNC-GNC 3.0/0.75 fibers surpassed the mechanical properties of MC 4.0 fibers but optically not transparent. The denser material in the dried solid state is suggested to enable CNC-GNCs to more tightly interact with the surrounding MC matrix and take advantage of the rigidness of the CNC-GNC hybrids. However, again the CNC-GNC additive fiber reinforcement (162 MPa maximum stress, 4.1 GPa Young's modulus) remained lower compared to pure CNCs (173 MPa maximum stress, 8.3 GPa Young´s modulus), even though it allowed slightly more ductile (43.8% maximum strain) fibers. In terms of maximum strength and stiffness, MC/CNC composite fibers were overall the best-preforming fibers yielding ultimate strengths around 173-190 MPa and stiffness of ca. 8.3 GPa. Moreover, the maximum strains remained in the range of 33-40% and well agreed with the earlier MC/CNC fiber study results.[81] The values are superior compared to other known fully cellulose-derived optical fibers.[53] The mechanical performance was observed to remain rather constant with all the tested solid contents, i.e., MC/CNC 1.0/0.25; MC/CNC 2.0/0.5; and MC/CNC 3.0/0.75, while the wet-strength (qualitatively assessed as the tendency of the fibers to break during the drying phase) and fiber

diameter correlated with the total mass. Importantly, a balance between the optimal mechanical performance available through CNCs and luminescence of the GNCs could be achieved through the addition of a low weight fraction of GNC-BSA to MC/CNC. Accordingly, a three-component system containing MC/CNC/GNC-BSA of 3.0/0.375/0.375 allowed luminescent fibers with good mechanical properties (155 MPa ultimate stress, 37.5% maximum strain, 5.0 GPa Young's modulus) close to those of MC/CNC fibers (**Table 1**, **Figure 6**c). The performance of various MC-based fibers was generally approximately in par or better than other known cellulose-based optical fibers.[53,54]

2.5 Optical fiber performance

Refractive indices of the MC and MC nanocomposites were determined from spin-coated thin films using ellipsometry (**Figure S13** and **S14**). The total internal reflection (TIR) phenomenon that traps the light signals within optical fibers and guarantees efficient signal transmission requires a surrounding medium (cladding) that has lower RI than the fiber core. Typically, in commercial optical fibers, this is ensured by a separate cladding layer on top of the core fiber. Here the MC fibers were prepared and manipulated as uniform refractive index core-only, i.e., their optical fiber performance directly relies on the relative optical characteristics of their surroundings. The refractive indices of the MC-based nanocomposites were in the range of ~1.48-1.50 (at λ = 632.8 nm) depending on the nanodopant type and concentration. Typically, pure nanodopants displayed higher RI, e.g., 1.51 for GNC-BSA and 1.56 for CNCs, due to their high crystallinity compared to amorphous and less dense pure MC (RI ~1.48). As a result, the refractive indices of the nanocomposites gained intermediate values, for instance, the addition of CNC-GNCs or CNCs to MC increased the observed RI from 1.48 of pure MC up to ~1.50 in the mixtures. Instead, the addition of GNC-BSA and GNC-GSH gave only a minor increase in RI compared to pure MC, since their densely packed cores occupy significantly smaller

volumes compared to CNCs and, thus, contribute less to the overall density of the nanocomposites.

Finally, representative samples of each fiber composition were studied for their potential for optical fiber and signal transmission efficiency. For the ease of manipulating and efficiently coupling the light into the fibers, compositions that produced thicker fibers were preferably selected, where possible. The fibers' ability to transmit light signals was determined by measuring the attenuation coefficients (α) of each fiber type with a cutback method using a continuous-wave red laser (λ = 662 nm) (**Figure 7** and **S15-S16**). Therein, a light signal with a known intensity was shone into the fiber from one end and the output power at different propagating lengths along the fiber was measured. Thus, the power of the output light at different fiber lengths was measured and the attenuation coefficients (α) were determined from the experimental data through a mathematical fitting. For materials with attenuation coefficient (α), the output intensity *I(z)* can be described with Beer-Lambert law (equation 1):

$$I(z) = I(0)e^{-\alpha z.} \qquad (1)$$

where *z* is the propagating length of the light along the fiber, *I(0)* the input light power, and *I(z)* the light power at different *z*. The experimentally determined attenuation coefficients (α) allowed quantitative comparison of the nanocomposites as optical fibers and the evaluation of the effects of each nanodopant similar to mechanical properties.

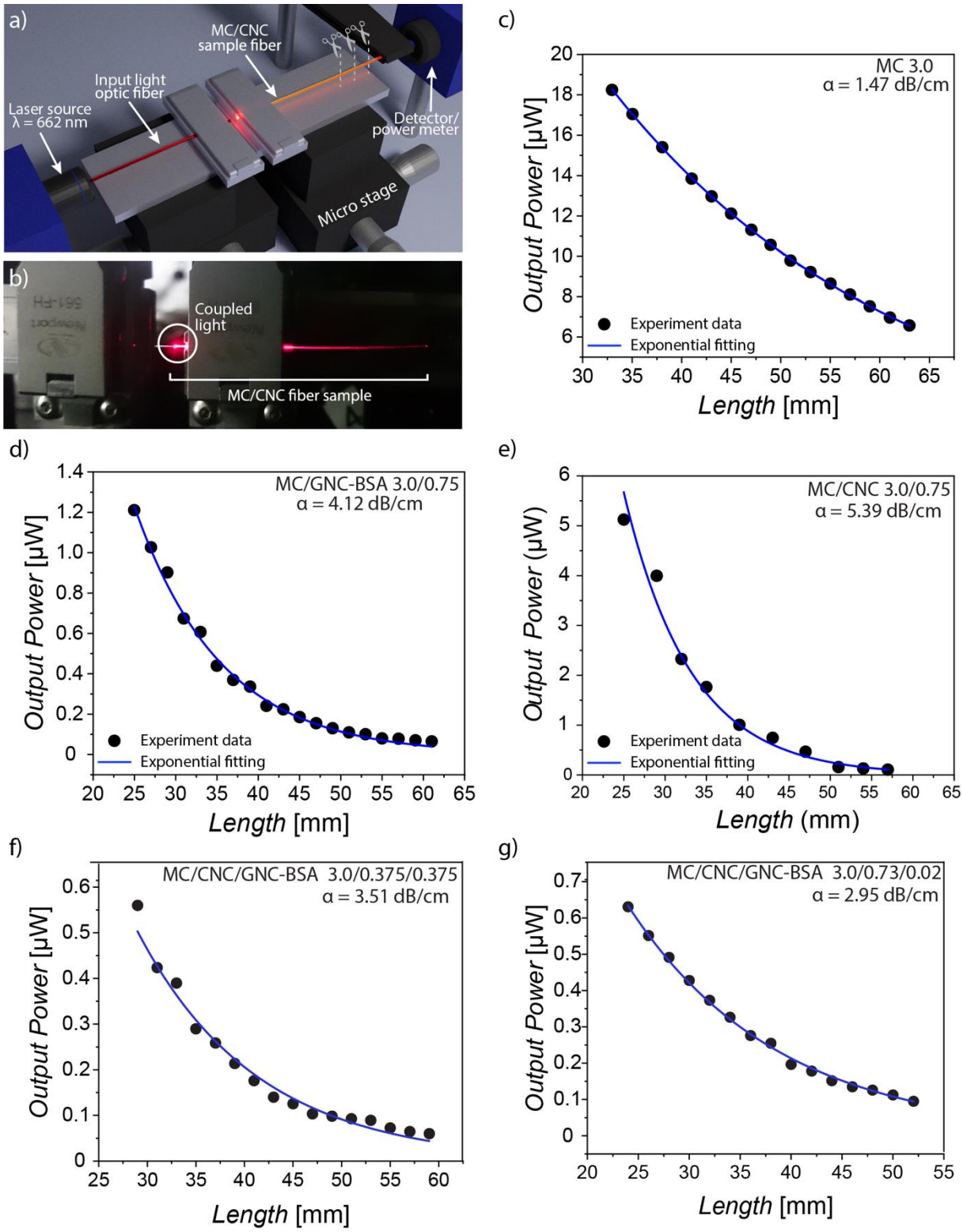

Figure 7. Attenuation coefficients of MC-based optical fibers. a) Schematic drawing of the cutback measurement method. Light is coupled to the sample fibers and output light intensity is measured repeatedly at different fiber lengths. b) Photograph of the coupled light propagating inside an MC/CNC 2.0/0.50 optic fiber sample during the cutback experiment. c-e) Representative experimental cutback data (black circles) and experimental fitting (blue solid line) of MC 3.0, MC/GNC-BSA and MC/CNC composite fibers.

Clear and glass-like pure MC 3.0 and MC 4.0 performed excellent wave propagation with attenuation coefficient. α of 1.47 dB cm^{-1} and 2.64 dB cm^{-1}, respectively. Even though the MC fiber performance is abysmal compared to the state-of-the-art commercial silica optical fibers designed for long-range communication (~0.2 dB km^{-1}), the attenuation coefficient of 1.47 dB cm^{-1} is on par or better than many biopolymer-based optical fibers reported in the literature.[54] It is important to note that the fibers studied in this work have no cladding layer (i.e., the surrounding air acts as a cladding). For instance, α of the relatively well-studied and well-performing silk optical waveguides generally fall in the range of 0.25-10.5 dB cm^{-1} depending on the waveguide type and environment.[25–34,53,54]

MC/GNC-BSA 3.0/0.75 were found relatively efficient as optical fibers and recorded α of 4.12 dB cm^{-1}, which was only slightly higher than MC 4.0. Thus, regardless of the addition of gold, the optical fiber capabilities were rather well retained. However, good-quality fibers were essential for the optical fiber performance as it was observed that any significant defects, such as small fiber-trapped air bubbles, or impurities easily resulted in highly absorbing hot spots that suppressed the propagating signals. The performance of MC/GNC-BSA was also compared against MC/BSA 3.0/0.75 control fiber, which had the α of 4.21 dB cm^{-1}, to further elucidate the role of gold. Based on the attenuation coefficients, the GNCs did not appear to significantly enhance absorption compared to pure BSA protein of similar mass. However, pure BSA additive tended to turn fibers slightly opaque, which was not observed with MC/GNC-BSA probably due to the more limited freedom and constricted structure of the GNC-bound BSA. The fibers prepared from MC/CNC-GNC 3.0/0.75 and MC/GNC-GSH 3.0/0.04 were tested unsuitable as optical fibers. They were opaque and enough light could not pass through to measure the attenuation coefficients.

The mechanically strongest MC/CNC fibers at all three tested compositions (1.0/0.25; 2.0/0.50; and 3.0/0.75) yielded α in the range of 3.95 -5.38 dB cm^{-1}. Similar to the trend with pure MC fibers, also here thicker fibers tended to yield higher attenuation coefficients (Figure

S17). Thus, the fiber thickness controlled by the total solid content also correlated with the observed attenuation coefficient. Even though the α of MC/CNC fibers shows higher optical loss than pure MC fibers, it can still be considered relatively good among biopolymeric optical fibers in general. It matches the performance of the most of the silk optical waveguides and also the other known fully cellulosic optical fibers reported in the literature. Remarkably, composite fibers prepared from MC/CNC/GNC-BSA of 3.0/0.375/0.375 and 3.0/0.73/0.02 showed attenuation coefficient of 3.5 dB cm^{-1} and 2.95 dB cm^{-1}, respectively. Importantly, these fibers also possess mechanical properties close to those of MC/CNC. Therefore, mechanically strong and ductile optical fibers with complementary properties are achieved.

Stretching of cellulosic fibers as a post-spinning processing method is known to align and reinforce the fiber structure, and it was probed here if the stretching would also affect the optical signal attenuation.[86,87] Thus, MC 3.0 and MC/CNC 3.0/0.75 fiber samples were gently stretched to ca. 10% after which the attenuation was measured. The attenuation coefficient of the stretched MC/CNC 3.0/0.75 fiber decreased from 5.39 to 4.34 dB cm^{-1} and is close to that of MC/GNC-BSA 3.0/0.75 fibers. In contrast, practically no difference was observed with the MC 3.0, whose α remained at ~1.47 dB cm^{-1}. It is suggested that the stretching improved the alignment of CNCs inside MC/CNC 3.0/0.75 fiber and mitigated the inherent defects in nanorod alignment originating, e.g. from the fiber flattening during the coagulation phase. Thus, stretching resulted in a more aligned structure, less scattering and improved signal transportation. In MC 3.0, the stretching effect remained negligible. The fiber did not contain larger rigid scattering objects similar to CNCs, i.e. the stretching of inherently homogeneous amorphous MC matrix did not produce as significant comparable overall structural changes.

2.7 Photostability and metal ion sensing of MC-GNC hybrid fibers

Since GNCs were added to the MC fibers through a simple mixing procedure without disrupting their structure, their inherent characteristic properties, such as intense fluorescence, were retained and effectively transferred to the nanocomposite fibers. When MC/GNC-BSA

was exposed for continuous UV-irradiation at 365 nm for 12 h, significantly lower photoluminescence bleaching was observed than the GNC-BSA. Thus, the incorporation of GNC-BSA into the MC matrix allowed improved photostability. A similar trend was also noticed for GNC-GSH and MC/GNC-GSH. The GNC-BSA is known to undergo fluorescence quenching in the presence of heavy metal ions, especially Hg^{2+}. To demonstrate whether the sensing abilities of GNC-BSA was retained after fiber extrusion and drying, the nanocomposite fibers were studied for Hg^{2+} sensing using MC/GNC-BSA 3.0/1.0, having slightly increased GNC-BSA content for additional sensitivity (**Figures 8** and **S18**).[66] The detection limit was found to be in the range of 1-10 mM upon fiber immersion in Hg^{2+} containing solution qualitatively detected as quenching of the photoluminescence under UV light within a few minutes (**Figure S18**).

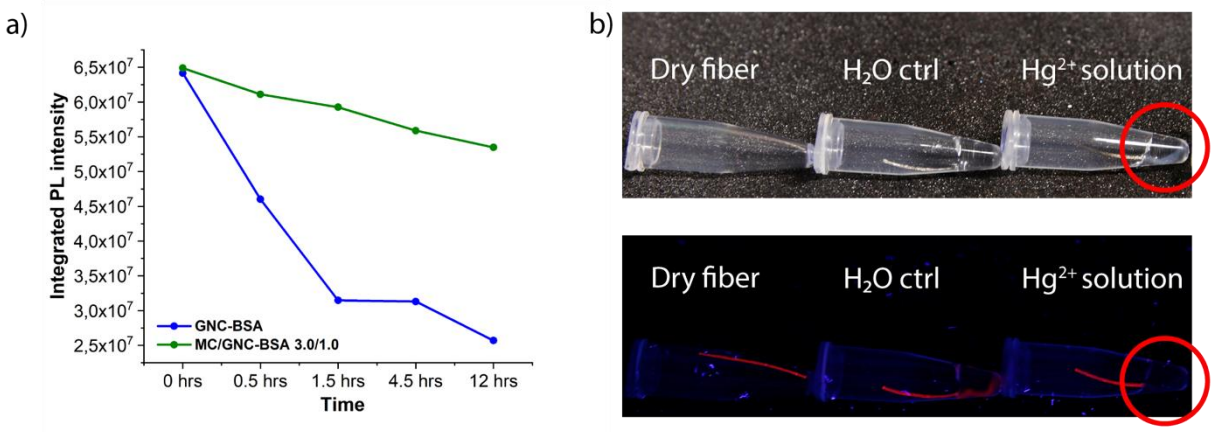

Figure 8. Functionalized MC/GNC fibers. a) MC matrix improved the photostability of the embedded photoluminescent GNC-BSAs. b) Mercury ion detection with MC/GNC-BSA 3.0/1.0 fibers. Three different fibers (from left to right: dry control sample, control fiber half-immersed in water, sensory fiber immersed in 10 mM aqueous Hg^{2+} solution). The possible accumulation of mercury on the fiber is seen within the red circle (top). Mercury-induced fluorescence quenching is detected in the part of the fiber immersed in the mercury ion containing solution highlighted with the red circle (bottom).

2.8 Fiber degradability under aqueous environment

The low optical loss and core-only nature of MC-based optical fibers would be well suited for biomedical applications where the required light propagation in tissue and organ-scale is some

tens of centimeters. Additionally, it is important for components inserted into living tissues to be degradable in a reasonable time scale to avoid unnecessary surgical removal operations and tissue damage. We studied the preliminary degradation behavior of MC-based optical fibers under an aqueous environment at two different temperatures. Accordingly, MC-CNC 2.0/0.5 fibers were fixed at two ends using carbon tape inside a petri dish and subsequently added deionized water, maintaining the temperature at either 22 °C or 37 °C. The wetting and appearance of the fibers were then followed until complete disintegration or for a time period of 6 hours (**Figure S19**). The fibers immersed in water at 22 °C completely degraded within 4 hours, showing highly hygroscopic behavior, which initially manifested as a rapid reversion to a more gel-like state. On the other hand, the fibers immersed in 37 °C survived substantially longer due to the LCST behavior of MC, which promotes gelation and increased stiffness through the formation of stiff fibrillar aggregates at temperatures close to and above 40 °C.[56] Even though some structural softening and fiber elongation were observed, the fiber diameter remained rather constant at 37 °C and the structural changes appeared to equilibrate into a stable hydrogel fiber. Moreover, the fibers could be picked up from the petri dish without breaking suggesting highly persisting structural intactness and strength regardless of the extreme humidity and wetting. This encourages the search for potential application targets in biological or other environments with elevated or tunable temperatures.

3.0 Conclusions

In summary, MC-based optical fibers studied in this work are highly competitive among the known biopolymeric optical waveguides. The MC matrix offers ample opportunity to incorporate various dopants under ambient conditions. The low attenuation coefficient of MC-based optical fibers, tunable mechanical and optical properties, and high photostability offers complimentary multifunctional fibers. The GNC-BSA and GNC-GSH additives provided mechanical reinforcement of solid fibers at surprisingly low 0.04% contents and provided fibers

with characteristic luminescence. Most importantly, the intrinsic optoelectronic properties and sensing capabilities of the GNCs were retained when incorporated into the MC matrix. At the same time, the composite fibers displayed high photostability against UV-irradiations. Thanks to the LCST characteristics of the MC matrix, fibers also showed temperature-dependent and tunable degradability in extreme wet conditions. The practically inexhaustible availability of cellulose, good mechanical and optical performance of the fibers, and the scalability and simplicity of the fiber spinning process make the MC-based fibers a tempting alternative, e.g. bio-optical silk fibers. The MC-based optical fibers pave the way for new, fully cellulose-based and environmentally friendly optical materials. The observed mechanical characteristics are also in stark contrast to the standard silica glass optical fibers that have been reported to express maximum stresses of ~1300 MPa (with polymer cladding) and 2600 MPa ("stripped" without cladding), maximum strain of ~5% and 3%, and Young's moduli of 22 GPa and 83 GPa, respectively. The respective moduli of toughness estimated from the stress-strain graphs were 34 MJ m^{-3} and 33 MJ m^{-3}. Therefore, especially the maximum strain of the different MC-based fibers significantly surpassed the commercial silica optical fibers, while the modulus of toughness was roughly equal or higher. As a general difference, silica fibers show practically pure elastic behavior until breakage without noticeable yielding. In contrast, the MC-based fibers expressed a clear yield point after a relatively short elastic response followed by a significant plastic deformation region. This highlights the softness and ductility of the MC-based fibers compared to the silica optical fibers. For example, it is beneficial in biological and medical applications, where optical components should be flexible and match the surrounding tissue's dynamic mechanical properties and motion to avoid breaking the component itself or mechanically damaging its soft surroundings. In general, the relatively high RI of 1.48-1.50 of the MC-based nanocomposites is excellent for, e.g., applications in biological contexts, where the RI of biological tissues generally lie in the range of 1.38-1.41, i.e., favorable for efficient TIR.

EXPERIMENTAL SECTION

Materials and Reagents

Methylcellulose (MC, MW 88,000, product no. M0512), $HAuCl_4.3H_2O$, reduced glutathione (GSH), bovine serum albumin (BSA), sodium hydroxide, metal salts used in the metal ion sensing experiment and sulfuric acid used in the CNC synthesis were purchased from Sigma-Aldrich and used as received. Aqueous solvents prepared from acetate salts of sodium (Na^+), Potassium (K^+), lead (Pb^{2+}), cobalt (Co^{2+}), mercury (Hg^{2+}), magnesium (Mg^{2+}), nickel (Ni^{2+}), zinc (Zn^{2+}), chlorides of lithium (Li^+), calcium (Ca^{2+}), copper (Cu^{2+}) and iron (Fe^{3+}), and nitrates of cadmium (Cd^{2+}) and aluminum (Al^{3+}) were used to screen specific ionic sensitivity of MC/GNC-BSA nanocomposite fibers. Whatman® 1 and Whatman® 541 filter papers and Spectra/Por® 1 standard dialysis tubing (MW cut-off 6 – 8 kDa) used in the CNC preparation were purchased from VWR. Absolute ethanol (99.7 vol/vol-% Etax Aa, Altia Inc.) was used in the coagulation bath (diluted to 96.0% v/v) during fiber spinning. Ultrapure MilliQ® water (18 Ω) was used in all experiments.

Synthesis of BSA encapsulated gold nanoclusters (GNC-BSA)

The synthesis of GNC-BSA was carried out following the reported procedure in the literature by Xie et al.[105] Briefly, 5 mL of 10 mM $HAuCl_4.3H_2O$ aqueous solution and 5 mL of aqueous BSA (50 mg/mL) solutions were prepared by dispersing in Milli Q (18 Ω) water and stored at 37 °C for 30 minutes. The aqueous solution of $HAuCl_4.3H_2O$ was then added to BSA solution under vigorous stirring at 37 °C. After 2 minutes, an aqueous solution of NaOH (1 M, 100 µL) was added to the above reaction mixture with constant stirring. A bright red dispersion of GNC-BSA was produced within 12 hours of the reaction at 37 °C. Finally, the solution was cooled at room temperature and stored at 4 °C for further use.

Synthesis of GSH functionalized gold nanoclusters (GNC-GSH)

The synthesis of GNC-GSH was performed according to a reported procedure by Luo et al.[106] Briefly, 500 µL (20 mM) of aqueous $HAuCl_4.3H_2O$ solution and 150 µL (100 mM) aqueous solution of glutathione were simultaneously added to 4.35 mL of Milli Q (18 Ω) water at 25 °C with gentle stirring over a magnetic stirrer. The stirring was continued for another 15 minutes until a colorless solution was obtained. The reaction mixture was heated at 70 °C for 24 hours in an oil bath with constant stirring of 500 rpm. Finally, the solution was cooled at room temperature and stored at 4 °C.

Synthesis of gold nanoclusters grafted over cellulose nanocrystals (CNC-GNC)

In a typical synthesis 500 µL (20 mM) aqueous solution of $HAuCl_4.3H_2O$ was mixed with 4.35 mL (14.5 mg/mL) of aqueous CNC dispersion with gentle stirring. The stirring was continued for 1 hour to allow the absorption of Au^{3+} over the negatively charged surface of CNC. To the reaction mixture, 150 µL (100 mM) aqueous solution of glutathione was added and the stirring was continued for another 15 minutes, followed by stirring at 70 °C for 24 hours. Finally, the solution was cooled to room temperature and the product was isolated by centrifugation at 4500 rpm for 3 hours. The supernatant was discarded and the CNC-GNC residue was immediately mixed with 5 mL of water followed by vertexing to obtain colloidal dispersion. Finally, the dispersion was stored at 4 °C for further use.

Preparation of Cellulose Nanocrystals (CNCs)

The cellulose nanocrystals (CNCs) were prepared from cotton filter paper (Whatman® 1) *via* acid hydrolysis according to a previously reported procedure.[107] In brief, mechanically ground filter paper powder (15 g) was hydrolyzed with sulfuric acid (64 w/w-%, 300 mL) under gentle agitation at 45 °C for 45 min. The reaction was quenched by diluting 10-fold with MQ H_2O and sedimented overnight, after which the clear supernatant was discarded. The remaining dispersion was washed with two centrifugation – pellet re-dispersion cycles followed by

dialysis against MQ H_2O until the conductivity of the dialysate remained below 5 µS cm^{-1}, and finally, a filtrated through Whatman® 541 filter paper. The ready-made CNCs were stored at + 4 °C until use. The solid content was determined gravimetrically, and the material was characterized with TEM, dynamic light scattering (DLS), zeta (ζ) potential measurements, and conductometric titration (Figure S1). Characterization data and experimental details are presented in the Supporting Information.

Preparation of Methylcellulose and methylcellulose-composite hydrogels

The desired amount of dry MC powder was dissolved in hot (~85 °C) MQ water according to the supplier's instructions and vigorously stirred until a homogeneous cloudy solution was achieved. The solution was cooled down in cold water bath (~10 °C) under constant mild shaking to hydrate the MC polymer chains and to promote even gelation until the material turned fully clear and transparent indicative of the gel state. Ready-made gels were stored at +4 °C until use. 2.0% (w/v; = 20 mg/mL), 3.0% and 4.0% pure MC gels were prepared. GNC, CNC-GNC and CNC dopants were pre-heated and added into the hot MC solution prior to the gelation, when needed, to guarantee homogeneous particle distribution within the gels. Gels relied fully on weak physical interactions of the components. MC-Bovine serum albumin control samples (without gold clusters) was prepared by mixing MC powder into pre-made and pre-heated BSA solution. Typically, MC composites with final concentration of 3.0% of MC and 0.75% (w/v) of a dopant were prepared to allow comparison based on the materials' total solid content. The gels were characterized with oscillatory rheological measurements and used for wet spinning of solid optical fibers. Furthermore, gels were used to prepare thin films for supportive optical and structural characterization of the bulk material. The details including the characterization methods are reported in the Supporting Information.

Fiber spinning and characterization

MC-based hydrogels were wet-spun into solid fibers by extrusion (1.8 mL/min constant flow speed) through a thin capillary tube (ø = 1 mm, length = 1 m) into a coagulation bath filled with ethanol (96.0 v/v-%) at room temperature (~22 °C).[90] The extrusion setup is schematically depicted in Figure 1. Before the extrusion, the gels were centrifuged (3000 rpm, 1-3 min) to remove possible gel-trapped air bubbles. The extrusion capillary was guided by hand so that the freshly extruded fiber did not overlap itself in the coagulation bath in order to avoid merging of the wet fiber segments. The selected flow speed allowed comfortable manual maneuverability, while remaining fast enough to produce good quality fibers. The nascent fiber was allowed to coagulate in ethanol for at least 25 min after which it was cut into ~8 cm long sample pieces and suspended to dry vertically fixed at both ends at ambient conditions (~22 °C, >15 h). The fibers are labelled and discussed in the text according to their initial hydrogel percentage (w/v) compositions. For example, MC 2.0 fiber has been spun from 2.0% (i.e. 20 mg/mL) MC hydrogel.

The mechanical properties of the fibers were studied by uniaxial tensile tests using a 5 kN tensile/compression module (Kammrath & Weiss GMbH, Germany) fitted with a 100 N load cell. The morphology and structure of the fibers was imaged with light microscopy and scanning electron microscopy (SEM). Degradation tests were used to study the durability of the fibers in various conditions. The experimental details on tensile tests, microscopy and degradation experiments are given in the Supporting Information.

To investigate the light guiding properties of the fibers, cutback method was used to assess the attenuation coefficients (α) of the fibers with different compositions following a reported literature procedure.[31]

Supporting Information

Supporting Information is available from the Wiley Online Library or from the author.

Acknowledgements

V.H. and S.C. contributed equally to this work. This work was carried out under the Academy of Finland´s Centre of Excellence in Molecular Engineering of Biosynthetic Hybrid Materials Research (HYBER, 2014-2019), ERC for Advanced grant (Driven 2017-2022), FinnCERES material cluster, Photonic Research and Innovation (PREIN) Flagship. Z.S. acknowledges funding from the Academy of Finland (Grant Nos. 325810, 312297, and 314810), PREIN (Grant No. 320167) and ERC grant (Grant No. 834742). S. C. acknowledges the Academy of Finland for project funding (Grant No. 310799). P.M. acknowledges the Jenny and Antti Wihuri Foundation (Centre for Young Synbio Scientists). V.H. acknowledges financial support from Walter Ahlström foundation and Finnish Foundation for Technology Promotion. We thank M. Junaid for useful discussions related to surface characterization. We acknowledge the provision of facilities and technical support by Aalto University OtaNano – Nanomicroscopy Center (Aalto-NMC).

Received: ((will be filled in by the editorial staff))
Revised: ((will be filled in by the editorial staff))
Published online: ((will be filled in by the editorial staff))

References

[1] Z. Liu, Z. F. Zhang, H.-Y. Tam, X. Tao, *Photonics* **2019**, *6*, 48.

[2] D. Shan, E. Gerhard, C. Zhang, J. W. Tierney, D. Xie, Z. Liu, J. Yang, *Bioactive Mater.* **2018**, *3*, 434.

[3] H. Ma, A. K.-Y. Jen, L. R. Dalton, *Adv. Mater.* **2002**, *14*, 1339.

[4] J. Böhm, J. Haußelt, P. Henzi, K. Litfin, T. Hanemann, *Adv. Eng. Mater.* **2004**, *6*, 52.

[5] K. Peters, *Smart Mater. Struct.* **2011**, *20*, 013002.

[6] P. Wang, Y. Wang, L. Tong, *Light Sci. and Appl.* **2013**, *2*, 102.

[7] A. Camposeo, F. di Benedetto, R. Stabile, A. A. R. Neves, R. Cingolani, D. Pisignano, *Small* **2009**, *5*, 562.

[8] J. Chen, P. Yang, C. Wang, S. Zhan, L. Zhang, Z. Huang, W. Li, C. Wang, Z. Jiang, C. Shao, *Nanoscale Res. Lett.* **2011**, *6*, 121.

[9] H. Liu, J. B. Edel, L. M. Bellan, H. G. Craighead, *Small* **2006**, *2*, 495.

[10] C. Grivas, J. Yang, M. B. J. Diemeer, A. Driessen, M. Pollnau, *Opt. Lett.* **2010**, *35*, 1983.

[11] M. Lu, H. Zhu, C. G. Bazuin, W. Peng, J. F. Masson, *ACS Sensors* **2019**, *4*, 613.

[12] J. Guo, B. Zhou, C. Yang, Q. Dai, L. Kong, *Adv. Funct. Mater.* **2019**, *29*, 1902898.

[13] M. Lanzarini-Lopes, B. Cruz, S. Garcia-Segura, A. Alum, M. Abbaszadegan, P. Westerhoff, *Environ. Sci. Technol.* **2019**, *53*, 10880.

[14] Nonappa, *Beilstein J. Nanotechnol.* **2020**, *11*, 533.

[15] J. B. Li, H. W. Liu, T. Fu, R. Wang, X. B. Zhang, W. Tan, *Trends Chem.* **2019**, *1*, 224.

[16] C. P. Montgomery, B. S. Murray, E. J. New, R. Pal, D. Parker, *Acc. Chem. Res.* **2009**, *42*, 925.

[17] U. Resch-Genger, M. Grabolle, S. Cavaliere-Jaricot, R. Nitschke, T. Nann, *Nat. Methods* **2008**, *5*, 763.

[18] M. Montalti, A. Cantelli, G. Battistelli, *Chem. Soc. Rev.* **2015**, *44*, 4853.

[19] A. Lacraz, M. Polis, A. Theodosiou, C. Koutsides, K. Kalli, *IEEE Photonics Technol. Lett.* **2015**, *27*, 693.

[20] D. L. Kaplan, R. Hartenstein, J. Sutter, *Appl. Environ. Microbiol.* **1979**, *38*, 551.

[21] M. C. J. Large, J. Moran, L. Ye, *Meas. Sci. Technol.* **2009**, *20*, 034014.

[22] K. Makino, Y. Akimoto, K. Koike, A. Kondo, A. Inoue, Y. Koike, *J. Light. Technol.* **2013**, *31*, 2407.

[23] A. Jain, A. H. J. Yang, D. Erickson, *Opt. Lett.* **2012**, *37*, 1472.

[24] M. Choi, M. Humar, S. Kim, S.-H. Yun, *Adv. Mater.* **2015**, *27*, 4081.

[25] J. Guo, X. Liu, N. Jiang, A. K. Yetisen, H. Yuk, C. Yang, A. Khademhosseini, X. Zhao, S.-H. Yun, *Adv. Mater.* **2016**, *28*, 10244.

[26] N. Jiang, R. Ahmed, A. A. Rifat, J. Guo, Y. Yin, Y. Montelongo, H. Butt, A. K. Yetisen, *Adv. Opti. Mater.* **2018**, *6*, 1701118.

[27] R. T. Chen, W. Phillips, T. Jannson, D. Pelka, *Opt. Lett.* **1989**, *14*, 892.

[28] A. K. Manocchi, P. Domachuk, F. G. Omenetto, H. Yi, *Biotechnol. Bioeng.* **2009**, *103*, 725.

[29] L. H. Chen, T. Li, C. C. Chan, R. Menon, P. Balamurali, M. Shaillender, B. Neu, X. M. Ang, P. Zu, W. C. Wong, K. C. Leong, *Sens. Actuators B Chem.* **2012**, *169*, 167.

[30] S. S. Voznesenskiy, A. A. Sergeev, A. Yu. Mironenko, S. Yu. Bratskaya, Yu. N. Kulchin, *Sens. Actuators B Chem.* **2013**, *188*, 482.

[31] A. Yu. Mironenko, A. A. Sergeev, A. E. Nazirov, E. B. Modin, S. S. Voznesenskiy, S. Yu. Bratskaya, *Sens. Actuators B Chem.* **2016**, *225*, 348.

[32] F. G. Omenetto, D. L. Kaplan, *Nat. Photonics* **2008**, *2*, 641.

[33] S. T. Parker, P. Domachuk, J. Amsden, J. Bressner, J. A. Lewis, D. L. Kaplan, F. G. Omenetto, *Adv. Mater.* **2009**, *21*, 2411.

[34] H. Tao, J. M. Kainerstorfer, S. M. Siebert, E. M. Pritchard, A. Sassaroli, B. J. B. Panilaitis, M. A. Brenckle, J. J. Amsden, J. Levitt, S. Fantini, D. L. Kaplan, F. G. Omenetto, *Proc. Natl. Acad. Sci.* **2012**, *109*, 19584.

[35] S. Kujala, A. Mannila, L. Karvonen, K. Kieu, Z. Sun, *Sci. Rep.* **2016**, *6*, 22358.

[36] S. Nizamoglu, M. C. Gather, M. Humar, M. Choi, S. Kim, K. S. Kim, S. K. Hahn, G. Scarcelli, M. Randolph, R. W. Redmond, S. H. Yun, *Nat. Commun.* **2016**, *7*, 10374.

[37] E. M. Heckman, J. G. Grote, F. K. Hopkins, P. P. Yaney, *Appl. Phys. Lett.* **2006**, *89*, 181116.

[38] W. Jung, B. Paulson, K. Choi, J. Y. Son, T. Nazari, S. H. Park, J. H. Kim, K. Oh, in *Optical Processes in Organic Materials and Nanostructures II* (Eds: M. Eich, J.-M. Nunzi, R. Jakubiak), Proc. SPIE 8827, **2013**.

[39] D. Klemm, B. Heublein, H.-P. Fink, A. Bohn, *Angew. Chem. Intl. Ed.* **2005**, *44*, 3358

[40] D. Li, L. Wang, *Opt. Commun.* **2010**, *283*, 2841.

[41] L. Peng, X. Yang, L. Yuan, L. Wang, E. Zhao, F. Tian, Y. Liu, *Opt. Commun.* **2011**, *284*, 4810.

[42] A. Lokman, S. Nodehi, M. Batumalay, H. Arof, H. Ahmad, S. W. Harun, *Microw. Opt. Technol. Lett.* **2014**, *56*, 380.

[43] A. Espinha, G. Guidetti, M. C. Serrano, B. Frka-Petesic, A. G. Dumanli, W. Y. Hamad, Á. Blanco, C. López, S. Vignolini, *ACS Appl. Mater. Interfaces* **2016**, *8*, 31935.

[44] G. Guidetti, S. Atifi, S. Vignolini, W. Y. Hamad, *Adv. Mater.* **2016**, *28*, 10042.

[45] F. I. Chowdhury, C. Dick, L. Meng, S. M. Mahpeykar, B. Ahvazi, X. Wang, *RSC Adv.* **2017**, *7*, 32436.

[46] B. Frka-Petesic, G. Guidetti, G. Kamita, S. Vignolini, *Adv. Mater.* **2017**, *29*, 1701469.

[47] Y.-D. He, Z.-L. Zhang, J. Xue, X.-H. Wang, F. Song, X.-L. Wang, L.-L. Zhu, Y.-Z. Wang, *ACS Appl. Mater. Interfaces* **2018**, *10*, 5805.

[48] M. S. Toivonen, O. D. Onelli, G. Jacucci, V. Lovikka, O. J. Rojas, O. Ikkala, S. Vignolini, *Adv. Mater.* **2018**, *30*, 1704050.

[49] O. Kose, A. Tran, L. Lewis, W. Y. Hamad, M. J. MacLachlan, *Nat. Commun.* **2019**, *10*, 510.

[50] T. H. Zhao, R. M. Parker, C. A. Williams, K. T. P. Lim, B. Frka-Petesic, S. Vignolini, *Adv. Funct. Mater.* **2019**, *29*, 1804531.

[51] E. Kontturi, P. Laaksonen, M. B. Linder, Nonappa, A. H. Gröschel, O. J. Rojas, O. Ikkala, *Adv. Mater*. **2018**, *30*, 1703779.

[52] K. Heise, E. Kontturi, Y. Allahverdiyeva, T. Tammelin, M. B. Linder, Nonappa, O. Ikkala, *Adv. Mater.* **2020**, 2004349.

[53] A. Dupuis, N. Guo, Y. Gao, N. Godbout, S. Lacroix, C. Dubois, M. Skorobogatiy, *Opt. Lett.* **2007**, *32*, 109.

[54] H. Orelma, A. Hokkanen, I. Leppänen, K. Kammiovirta, M. Kapulainen, A. Harlin, *Cellulose* **2020**, 27. 1543.

[55] T. L. Rogers, D. Wallick, *Drug Dev. Ind. Pharm.* **2012**, *38*, 129.

[56] P. L. Nasatto, F. Pignon, J. L. M. Silveira, M. E. R. Duarte, M. D. Noseda, M. Rinaudo, *Polymers* **2015**, *7*, 777.

[57] H. C. Arca, L. I. Mosquera-Giraldo, V. Bi, D. Xu, L. S. Taylor, K. J. Edgar, *Biomacromolecules* **2018**, *19*, 2351.

[58] L. Li, *Macromolecules* **2002**, *35*, 5990.

[59] J. P. A. Fairclough, H. Yu, O. Kelly, A. J. Ryan, R. L. Sammler, M. Radler, *Langmuir* **2012**, *28*, 10551.

[60] S. A. Arvidson, J. R. Lott, J. W. McAllister, J. Zhang, F. S. Bates, T. P. Lodge, R. L. Sammler, Y. Li, M. Brackhagen, *Macromolecules* **2013**, *46*, 300.

[61] R. Jin, C. Zeng, M. Zhou, Y. Chen, *Chem. Rev.* **2016**, *116*, 10346.

[62] I. Chakraborty, T. Pradeep, *Chem. Rev.* **2017**, *117*, 8208.

[63] Nonappa, T. Lahtinen, Johannes. S. Haataja, T.-R. Tero, H. Häkkinen, O. Ikkala, *Angew. Chem. Intl. Ed.* **2016**, *55*, 16035.

[64] Nonappa, O. Ikkala, *Adv. Funct. Mater.***2018**, *28*, 1704328.

[65] L. Zhang, E. Wang, *Nano Today* **2014**, *9*, 132.

[66] N. Mohammed, A. Baidya, V. Murugesan, A. A. Kumar, M. A. Ganayee, J. S. Mohanty, K. C. Tam, T. Pradeep, *ACS Sustain. Chem. Eng.* **2016**, *4*, 6167.

[67] A. Senthamizhan, A. Celebioglu, T. Uyar, *J. Mater. Chem. A* **2014**, *2*, 12717.

[68] U. S. Akshath, P. Bhatt, S. A. Singh, *J. Fluoresc.* **2020**, *30*, 537.

[69] K. Chaudhari, P. L. Xavier, T. Pradeep, *ACS Nano* **2011**, *5*, 8816.

[70] G. Li, R. Jin, *Acc. Chem. Res.* **2013**, *46*, 1749.

[71] Y. S. Chen, P. V. Kamat, *J. Am. Chem. Soc.* **2014**, *136*, 6075.

[72] S. Chandra, Nonappa, G. Beaune, A. Som, S. Zhou, J. Lahtinen, H. Jiang, J. V. I. Timonen, O. Ikkala, R. H. A. Ras, *Adv. Opt. Mater.* **2019**, *7*, 1900620.

[73] S. H. Yau, O. Varnavski, T. Goodson, *Acc. Chem. Res.* **2013**,*46*, 1506.

[74] Y. Z. Lu, W. Chen W. *Chem. Soc. Rev.* **2012**, *41*, 3594.

[75] N. Goswami, F. Lin, Y. Liu, D. T. Leong, J. Xie, *Chem. Mater*. **2016**, *28*, 4009.

[76] K. Pyo, V. D. Thanthirige, K. Kwak, P. Pandurangan, G. Ramakrishna, D. Leev, *J. Am. Chem. Soc.* **2015**, *137*, 25, 8244.

[77] X. Kang, M. Zhu, *Chem. Soc. Rev*. **2019**, *48*, 2422.

[78] K. Chaudhari, P. L. Xavier, T. Pradeep *ACS Nano* **2011**, *5*, 11, 8816.

[79] P. L. Xavier, K. Chaudhari, A. Baksi, T. Pradeep, *Nano Rev.* **2012**, *3*, 14767.

[80] V. Hynninen, S. Hietala, J. R. McKee, L. Murtomäki, O. J. Rojas, O. Ikkala, Nonappa, *Biomacromolecules* **2018**, *19*, 2795.

[81] V. Hynninen, P. Mohammadi, W. Wagermaier, S. Hietala, M. B. Linder, O. Ikkala, Nonappa, *Eur. Polym. J.* **2019**, *112*, 334.

[82] P. Mohammadi, M. S. Toivonen, O. Ikkala, W. Wagermaier, M. B. Linder, *Sci. Rep.* **2017**, *7*, 11860.

[83] S. C. Baxter, C. T. Robinson, *Compos. Sci. Technol.* **2011**, *71*, 1273.

[84] A. Pakzad, J. Simonsen, R. S. Yassar, *Compos. Sci. Technol.* **2012**, *72*, 314.

[85] J. Sapkota, J. C. Martinez Garcia, M. Lattuada, *J. Appl. Polym. Sci.* **2017**, *134*, 45254.

[86] J. G. Torres-Rendon, F. H. Schacher, S. Ifuku, A. Walther, *Biomacromolecules* **2014**, *15*, 2709.

[87] H. C. Kim, D. Kim, J. Y. Lee, L. Zhai, J. Kim, *Int. J. Precis. Eng. and Manuf.-Green Tech.* **2019**, *6*, 567.

[88] J. Xie, Y. Zheng, J. Y. Ying, *J. Am. Chem. Soc.* **2009**, *131*, 888.

[89] Z. Luo, X. Yuan, Y. Yu, Q. Zhang, D. T. Leong, J. Y. Lee, J. Xie, *J. Am. Chem. Soc.* **2012**, *134*, 16662.

[90] V. Chean, E. Robin, R. El Abdi, J.-C. Sangleboeuf, *EPJ Web Conf.* **2010**, *6*, 34002.

Table of content entry

V. Hynninen, S. Chandra, S. Das, M. Amini, Y. Dai, S. Lepikko, P. Mohammadi, S. Hietala, R. H. A. Ras, Z. Sun, O. Ikkala*, Nonappa*

Luminescent Gold Nanocluster-Methylcellulose Hybrid Optical Fibers with Low Attenuation Coefficient and High Photostability

Simple extrusion of shear-thinning methylcellulose and gold nanoclusters (GNCs) composite hydrogels enables mechanically and optically tunable biopolymeric optical fibers. The resulting composite fibers display low attenuation coefficient making them suitable for application in short-distance optical fibers.